Protein Science (1993), *2*, 2085–2094. Cambridge University Press. Printed in the USA.

Fluorescence characterization of Trp 21 in rat glutathione *S*-transferase 1-1: Microconformational changes induced by *S*-hexyl glutathione

REGINA W. WANG,[1] ANDREW W. BIRD,[2] DEBORAH J. NEWTON,[1]
ANTHONY Y. H. LU,[1] AND WILLIAM M. ATKINS[2]

[1] Department of Animal & Exploratory Drug Metabolism, Merck Research Laboratories, P.O. Box 2000, Rahway, New Jersey 07065
[2] Department of Medicinal Chemistry, BG-20, University of Washington, Seattle, Washington 98195

(RECEIVED April 13, 1993; ACCEPTED August 17, 1993)

Abstract

The glutathione *S*-transferase (GST) isoenzyme A1-1 from rat contains a single tryptophan, Trp 21, which is expected to lie within α-helix 1 based on comparison with the X-ray crystal structures of the pi- and mu-class enzymes. Steady-state and multifrequency phase/modulation fluorescence studies have been performed in order to characterize the fluorescence parameters of this tryptophan and to document ligand-induced conformational changes in this region of the protein. Addition of *S*-hexyl glutathione to GST isoenzyme A1-1 causes an increase in the steady-state fluorescence intensity, whereas addition of the substrate glutathione has no effect. Frequency-domain excited-state lifetime measurements indicate that Trp 21 exhibits three exponential decays in substrate-free GST. In the presence of *S*-hexyl glutathione, the data are also best described by the sum of three exponential decays, but the recovered lifetime values change. For the substrate-free protein, the short lifetime component contributes 9–16% of the total intensity at four wavelengths spanning the emission. The fractional intensity of this lifetime component is decreased to less than 3% in the presence of *S*-hexyl glutathione. Steady-state quenching experiments indicate that Trp 21 is insensitive to quenching by iodide, but it is readily quenched by acrylamide. Acrylamide-quenching experiments at several emission wavelengths indicate that the long-wavelength components become quenched more easily in the presence of *S*-hexyl glutathione. Differential fluorescence polarization measurements also have been performed, and the data describe the sum of two anisotropy decay rates. The recovered rotational correlation times for this model are 26 ns and 0.81 ns, which can be attributed to global motion of the protein dimer, and fast local motion of the tryptophan side chain. These results demonstrate that regions of GST that are not in direct contact with bound substrates are mobile and undergo microconformational rearrangement when the "H-site" is occupied.

Keywords: anisotropy decay; glutathione *S*-transferase; protein dynamics; time-resolved fluorescence; tryptophan fluorescence

Reprint requests to: William M. Atkins, Department of Medicinal Chemistry, BG-20, University of Washington, Seattle, Washington 98195.

Abbreviations: GST, glutathione *S*-transferase; GSH, glutathione; CDNB, 1-chloro-2,4-dinitrobenzene; DAS, decay-associated spectra; Ksv_i, the apparent Stern–Volmer quenching constant for an individual component of a mixture of fluorophores; MOPS, 3-(*N*-morpholino)propane-sulfonic acid; SAS, species-associated spectra. Prefixes A, P, and M before numbers such as 1-1 or 3-3 refer to the gene classes alpha, pi, and mu, respectively. The numbers refer to the individual subunits that comprise a particular isoenzyme within the classes. For example, the rat A1-1 refers to the alpha-class isoenzyme 1-1, referred to previously as the YaYa isoenzyme. The system referring to structural domains of these proteins is that of Ji et al. (1992). Starting from the N-terminus, the first and second α-helices are helix 1 and helix 2, and the first and second β-sheets are β-sheet 1 and β-sheet 2. This makes helix-1 equivalent to helix-A, according to Reinemer et al. (1991). See these references for more detail.

The glutathione *S*-transferases (EC 2.5.1.18) are a family of conjugative enzymes that catalyze the nucleophilic addition of glutathione to a wide range of endogenous substrates, xenobiotics, and carcinogens (Mannervik & Danielson, 1988; Coles & Ketterer, 1990). The cytosolic isozymes represent four distinct gene classes, designated alpha, mu, pi, and theta (Mannervik, 1985; Pickett & Lu, 1989; Meyer et al., 1991). The enzymes produced from these gene classes are distinguished by their substrate specificities and primary amino acid sequence homologies. Recently, X-ray crystal structures have indicated that pi- and mu-class GSTs with different ligands bound have nearly identical three-dimensional topologies (Reinemer

et al., 1991, 1992; Ji et al., 1992). NMR studies also have demonstrated the similarity in structure between these classes of GSTs (Penington & Rule, 1992). Individual subunits of GSTs from both of these classes consist of two distinct domains. The N-terminal domain (domain I) contains both β-sheet and α-helical elements, whereas the larger C-terminal domain (domain II) contains no β-sheet structure. The glutathione-binding site ("G-site") lies nearly completely within the N-terminal domain of each subunit, yet includes a single salt bridge between GSH bound to one subunit and an evolutionarily conserved aspartate in the adjacent subunit (Wang et al., 1992a; Kong et al., 1993). Notably, the GSH-binding site lies near the N-termini of α-helices 1 and 3, and it has been suggested that the resulting helical dipoles may play an electrostatic role in GSH binding (Graminski et al., 1989; Reinemer et al., 1991). The binding site for the electrophilic substrates that are conjugated to GSH, the "H-site," is also localized partly within the N-terminal domain. However, several residues within the C-terminal domain contribute to this binding pocket. Construction of chimeric GSTs has demonstrated that the H-site specificity reflects a complex interaction between N-terminal and C-terminal regions of the protein (Zhang & Armstrong, 1990). Although a great deal of structural data concerning ligand-bound GSTs are now available, no X-ray crystal structure has been published for any GST in the absence of substrate.

Details of the chemical mechanism of GSH conjugation have been obtained from site-directed mutants as well as spectroscopic techniques (Graminski et al., 1989; Armstrong, 1991; Liu et al., 1992). Although the catalytic roles of specific residues have been demonstrated, ligand-induced conformational changes have not been characterized in detail, and active-site reorganization may be required as the reaction progresses from the substrate-free form of the enzyme to the final product complex. Thus, the conformational dynamics associated with ligand binding to GSTs remain undefined. Furthermore, the solution dynamics of GST proteins have not been studied, although the crystallographically determined temperature factors indicate that there are distinct regions of localized side-chain mobility surrounding a relatively static protein core (Ji et al., 1992). In order to interpret the free-energy profile of the enzyme-catalyzed reaction in molecular terms, and to effectively design class-specific inhibitors of GST, it is necessary to document structural and dynamic changes that take place when the substrate-free enzymes bind substrates, inhibitors, and products. The objective of these studies was to determine whether such conformational dynamics are important for the function of GST.

Tryptophan residues provide valuable intrinsic probes of localized protein motion and of protein–substrate interactions (Lakowicz, 1989; Royer et al., 1990; Harris & Hudson, 1991). Indeed, steady-state fluorescence studies have demonstrated that a tryptophan residue is involved directly in binding of GSH to a pi-class GST (Caccuri et al., 1991; Nishihara et al., 1992). These results are consistent with the X-ray structure of the pi-class enzyme, which indicates that Trp 38 is in direct contact with GSH analogues bound at the G-site (Reinemer et al., 1991, 1992). In contrast to many mu-class and pi-class GSTs, which contain two or more tryptophans, the rat isoenzyme A1-1 has a single tryptophan residue. This is Trp 21, which is conserved only in alpha-class GSTs and is therefore not expected to contact GSH directly at the active site (Mannervik & Danielson, 1988). Trp 21 of the A1-1 isoenzyme would be expected to lie near the C-terminus of α-helix 1, based on the available crystal structures. Because this is the only tryptophan contained within this isoenzyme, it provides a specific spectroscopic probe of conformational dynamics of an alpha-class GST, and in particular, of the α-helix that begins near the GSH-binding site. We report time-resolved and steady-state fluorescence experiments which demonstrate that this side chain exhibits fast rotational motion and that α-helix 1 undergoes a microconformational change when *S*-hexyl GSH binds to the substrate-free A1-1 GST isolated from rat. This is an initial characterization of the relationship between dynamics and function of the GST family of proteins.

Results

Steady-state fluorescence and lifetime measurements

The steady-state emission spectrum of rat A 1-1 GST exhibits a maximum at 329 nm at pH 7.4, 25 °C, in the absence of substrate, when the excitation wavelength is 295 nm. Addition of saturating concentrations of GSH (400 μM) has no detectable effect on the steady-state intensity or emission wavelength maximum. However, addition of saturating *S*-hexyl GSH (200 μM) results in a modest increase in intensity (13%, Fig. 1). This is noteworthy because Trp 21 is not expected to contribute directly to the GSH-binding site or the H-site, based on the crystal structures of the pi- and mu-class enzymes. This result suggested that when ligands bind to the H-site, or during formation of the transition state for GSH conjugation to electrophilic substrates, the enzyme undergoes a conformational change that does not occur when GSH binds to the active site. Because this isoenzyme has a single tryptophan, this spectroscopic change can be correlated to structural changes within the region of Trp 21. This prompted a more detailed examination using time-resolved, frequency-domain, excited-state lifetime measurements. The phase and modulation data for 12 modulation frequencies of excitation light are shown in Figure 2. There is a clear shift in the frequency response of Trp 21 toward lower frequencies when *S*-hexyl GSH is added, indicating a longer average excited-state lifetime. This is observed at each of the emission wavelengths stud-

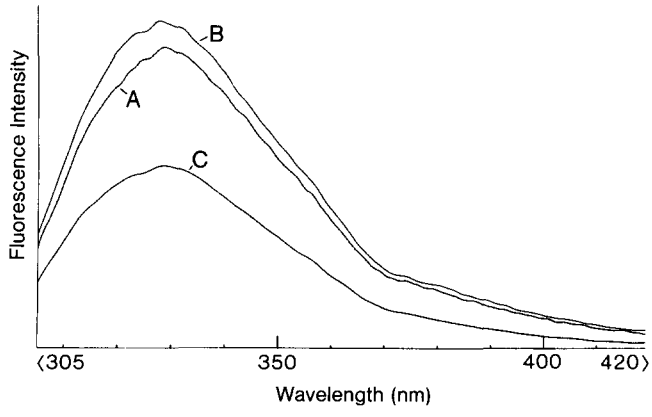

Fig. 1. Steady-state emission spectra of rat A1-1 GST. **A:** 5 μM substrate-free enzyme. **B:** After addition of 200 μM *S*-hexyl GSH. **C:** Substrate-free protein after addition of 150 mM acrylamide. Excitation wavelength was 295 nm.

ied. Several physical models for the excited-state fluorescence decay were tested to determine which best described the data. A sum of exponentials is the assumed decay scheme. Global analysis of the phase and modulation data indicated that Trp 21 exhibits at least three excited-state lifetimes in both the substrate-free protein and in the presence of *S*-hexyl GSH; single and double exponential-decay models afforded significantly higher χ^2 values and weighted residuals that were dispersed nonrandomly. Similarly, analysis of the data as continuous distributions of lifetime values did not significantly improve the fit of the data to the model. Complex combinations of discrete lifetime components and distributed components does not improve the χ^2 value or the distribution of weighted residuals. Thus, although tryptophans in many proteins have been shown to be described by distributions of excited-state lifetimes, we have treated Trp 21 of rat A1-1 GST as having three discrete lifetimes (Alcala et al., 1987). The recovered lifetime values and fractional intensities are summarized in Table 1. The upper and lower limits of the recovered lifetime values determined by rigorous error analysis (Globals Unlimited®) are indicated by the ± entries. In the model shown, the lifetime value of each component is constrained to remain the same at each emission wavelength, and the observed heterogeneous decay kinetics are assumed to result from ground-state heterogeneity. When the lifetime values are allowed to vary as a function of emission wavelength, the global χ^2 does not change significantly even though there are fewer constraints. The physical model in which the heterogeneous decay kinetics of single tryptophan proteins result from ground-state heterogeneity has been accepted widely (Beechem et al., 1983; Hutnik & Szabo, 1989; Royer et al., 1993). Furthermore, negative preexponential factors were not recovered, and nonexponential decay kinetics were not observed under any conditions.

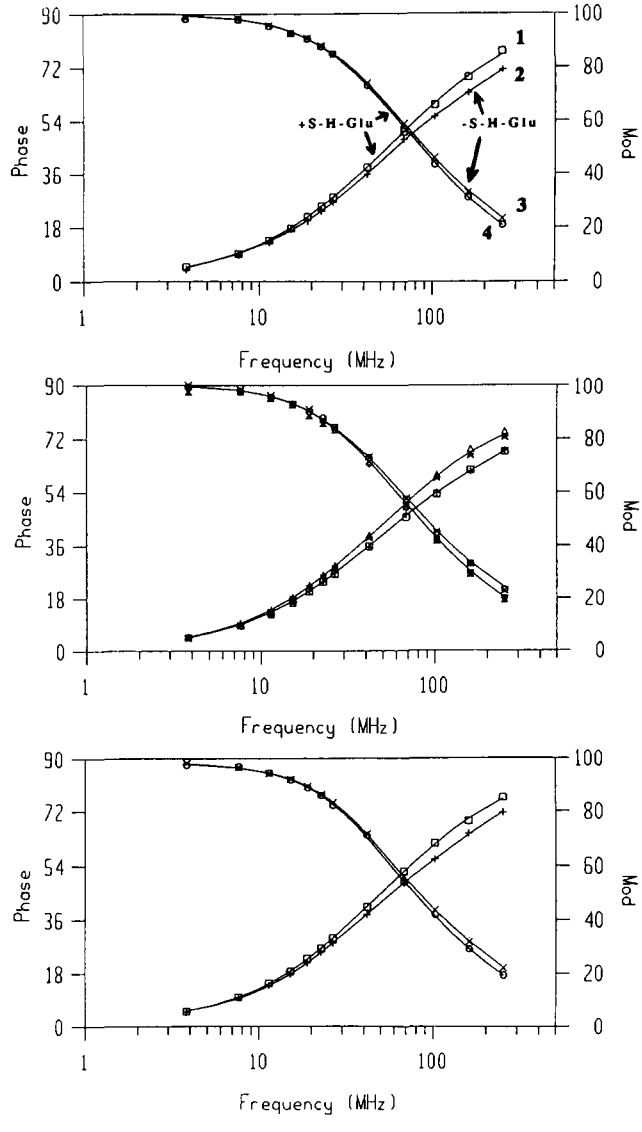

Fig. 2. Phase and modulation data for A1-1 GST in the presence and absence of *S*-hexyl GSH. The phase angles (squares, crosses, triangles, stars) and modulation ratios (circles, x's) were measured at 12 modulation frequencies as described in the Materials and methods. Data for three emission wavelengths are shown. Top, 320 nm; middle, 330 nm, two data sets for phase angles and two data sets for modulation ratios; bottom, 340 nm. In the top panel, curves 1 and 4 correspond to data in the presence of *S*-hexyl GSH (+*S*-H-Glu). Curves 2 and 3 represent data in the absence of the inhibitor (−*S*-H-Glu). These trends are maintained in the middle and bottom panels.

Thus, excited-state processes were not detected, and ground-state heterogeneity provides a simple model consistent with the results. This model is limited by experimental resolution, and there may be more than three conformational substates sampled by Trp 21 that cannot be resolved by this technique, i.e., the species-associated spectra of each lifetime component may represent an average of several substates with a single apparent excited-state lifetime.

Table 1. *Fluorescence lifetimes and fractional intensities of Trp 21 in the absence and presence of S-hexyl glutathione*

Ligand state[a]	Global χ^2	Lifetime[b] (ns)	Fractional intensity[c]: 320, 330, 340, 360, 380 nm
No *S*-hexyl	1.865	6.74 ± 0.32/0.68	0.162, 0.215, 0.236, 0.307, 0.374
		2.93 ± 0.34/0.38	0.720, 0.628, 0.653, 0.586, 0.533
		0.814 ± 0.30/0.41	0.118, 0.157, 0.111, 0.107, 0.093
+*S*-hexyl GSH	2.095	5.23 ± 0.86/0.41	0.415, 0.487, 0.512, 0.603
		2.25 ± 0.79/0.60	0.585, 0.479, 0.480, 0.390
		0.49 ± 0.84/0.67	0.000, 0.033, 0.008, 0.007

[a] Samples were 5 μM GST, 50 mM MOPS, pH 7.5, 25 °C. The *S*-hexyl GSH was 200 μM.
[b] The indicated errors are the high and low limits at the 67% confidence interval as determined by rigorous error analysis provided in Globals Unlimited®.
[c] Five emission wavelengths were studied for the substrate-free enzyme and four wavelengths were studied for the *S*-hexyl GSH complex. For direct comparison, the 380-nm data here are omitted from the model shown in Figure 3.

In the absence of substrate, the long lifetime component (6.74 ns) is relatively red-shifted compared to the median component (2.93 ns). The short lifetime component, 0.81 ns, demonstrates little wavelength dependence. In the presence of *S*-hexyl GSH, the recovered lifetime values are 5.23 ns, 2.25 ns, and 0.49 ns. It is striking that the short lifetime component present in the substrate-free protein is nearly absent, and there is a correspondingly greater fraction of the long lifetime component. Although there is only 1–3% of the short lifetime component in the ligand-bound protein, attempts to fit the data to the sum of two exponentials raised the χ^2 value significantly to 3.48. The results summarized in Table 1 are depicted as SAS in Figure 3. For the case of ground-state heterogeneity, decay-associated spectra and SAS are readily interconvertible.

The model summarized in Table 1 assumes that the lifetime components of the substrate-free GST are independent from the lifetime components of the *S*-hexyl GSH-bound enzyme. Consideration must be given to whether the lifetime values recovered in each analysis are the same and only the fractional intensities differ between ligand states, or whether the ligand results in new excited-state lifetimes. Therefore, the data were analyzed with the three lifetime components constrained to be the same in both ligand states. However, the data fit poorly to the model with these constraints ($\chi^2 = 5.01$). On the other hand, the confidence limits resulting from rigorous error analysis for the individual excited-state lifetime values indicate that the short lifetime and the median lifetime values are not completely resolved between ligand states. Because the long lifetime components are well resolved when the substrate-free and *S*-hexyl GSH-bound proteins are compared in a single global analysis, we have shown the model depicted in Figure 3, which indicates different lifetime values for the two ligand states. The model in which these long lifetime components represent different microconformational states associated with the presence or absence of ligand is supported by the steady-state quenching experiments described below.

Fluorescence quenching

The excited-state lifetime measurements indicate that Trp 21 adopts new microconformational states upon addition of *S*-hexyl GSH. In order to examine the nature of this change in more detail, steady-state solute quenching

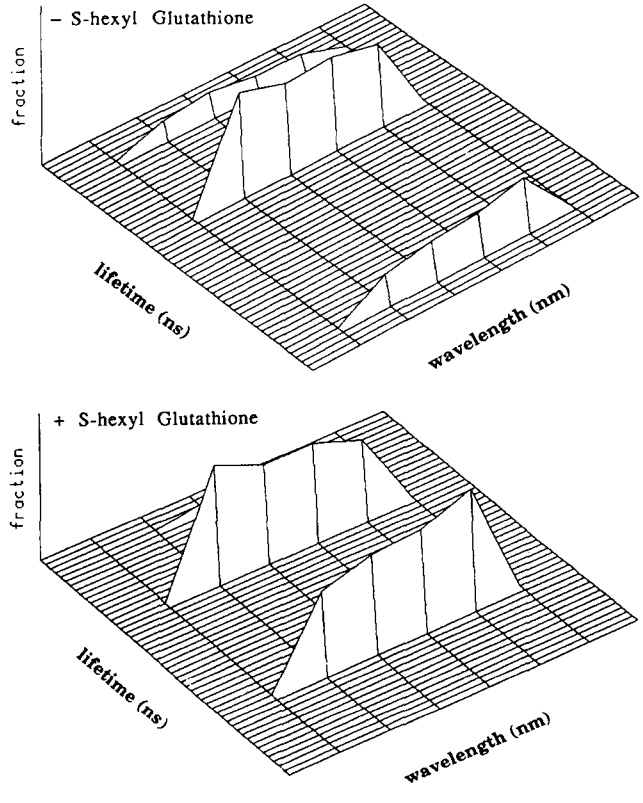

Fig. 3. SAS for A1-1 GSH *S*-transferase in the presence and absence of 200 μM *S*-hexyl GSH. Samples were 10 μM GST. The wavelength axis includes data for four emission wavelengths, 320, 330, 340, and 360 nm. The recovered values for the excited-state lifetimes in the presence and absence of *S*-hexyl GSH are summarized in Table 1. For SAS, the total intensity of the summed lifetime components is normalized to 1 at each wavelength. Top, no *S*-hexyl GSH; bottom, 200 μM *S*-hexyl GSH.

experiments were performed. Specifically, iodide ion and acrylamide were used to probe the environment of Trp 21. Iodide has been used extensively to quench tryptophans that are in polar regions of proteins, particularly near positively charged sites (Stayton & Sligar, 1990; Eftink, 1991). Trp 21 of rat A1-1 GST is relatively insensitive to iodide quenching. Negligible quenching was observed at 200 mM KI. When higher concentrations of iodide were used (400 mM), slow time-dependent changes in the fluorescence spectra were observed. Therefore, a Stern-Volmer quenching constant could not be determined. The cause of this gradual change in fluorescence properties at high KI concentrations was not examined in further detail, but the results indicate clearly the relative insensitivity of Trp 21 to quenching by iodide.

In contrast, Trp 21 is readily quenched by acrylamide, and the wavelength dependence of the apparent quenching constants differs dramatically between the substrate-free and *S*-hexyl GSH-bound proteins (Fig. 4). Quenching

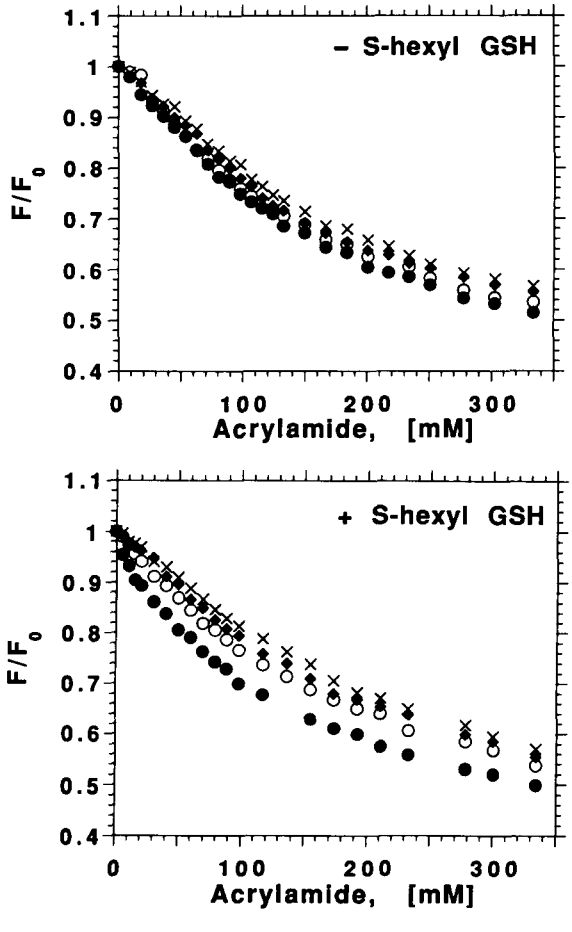

Fig. 4. Modified Stern-Volmer plots for steady-state quenching of A1-1 GST by acrylamide. The plots correspond to four emission wavelengths: crosses, 320 nm; closed diamonds, 330 nm; open circles, 360 nm; closed circles, 380 nm. Conditions were as described in the Materials and methods.

by acrylamide was examined at 320, 330, 360, and 380 nm. At low acrylamide concentrations, the *S*-hexyl GSH-bound enzyme demonstrates much greater wavelength dependence than the substrate-free protein. This wavelength dependence presumably reflects ground-state heterogeneity, where the individual lifetime components are quenched differentially by acrylamide (Eftink, 1991). The data suggest that the difference in quenching constants for the individual lifetime components, Ksv_i, or their fractional intensities, f_i, is more pronounced in the the presence of *S*-hexyl GSH than in its absence. Assuming that ground-state heterogeneity provides the observed wavelength dependence of the apparent *Ksv* values (Eftink, 1991), the data shown in these modified Stern-Volmer plots have also been analyzed by nonlinear regression, using the equation $F/F_0 = \sum f_i/(1 + Ksv_i Q)$. Unique solutions of this analysis were obtained for the data at the extreme wavelengths, 320 nm and 380 nm. At intermediate wavelengths, unique solutions were not recovered, and several fits to the data were indistinguishable based on standard statistical criteria.

Static quenching mechanisms also were considered. No upward curvature is apparent in standard Stern-Volmer plots. Nonlinear regression using an equation with a static quenching term was also performed, but this did not improve the fit of these data and did not yield unique solutions. Furthermore, the static-quenching volume elements (V_i) recovered from this analysis were often negative. Therefore, if a static-quenching mechanism is operative, it is a minor component and we report results obtained assuming that only dynamic quenching is significant kinetically. Also, attempts to fit the quenching data to the sum of three discrete components with individual Ksv_i values did not yield better correspondence between the data and the model. Given the small contribution of a very short lifetime component for each ligand state of the protein (<11%), it is likely that this component does not contribute to the observed solute quenching by a dynamic-quenching mechanism. Thus, the quenching data fit well to a model described by the sum of two components, whereas the lifetime analysis required a third component for a satisfactory excited-state decay model.

The recovered quenching parameters for emission at 320 nm and 380 nm are summarized in Table 2, and they provide additional evidence that *S*-hexyl GSH causes a microconformational change at the C-terminal end of helix 1. Furthermore, the spectrum of GST quenched by acrylamide is slightly blue-shifted (2–3 nm) compared to the original spectrum (Fig. 1). This effect is readily apparent when normalized spectra of protein in the presence of varying concentrations of acrylamide are compared (not shown). This is particularly noteworthy when the lifetime data are considered because addition of *S*-hexyl GSH to GST results in a redistribution of lifetime components that have different wavelength dependences (Fig. 3). If the red-shifted, long lifetime component is quenched more

Table 2. *Steady-state acrylamide quenching of Trp 21*

Ligand state[a]	320 nm[b]				380 nm			
	f_1	Ksv_1 (M^{-1})	f_2	Ksv_2 (M^{-1})	f_1	Ksv_1 (M^{-1})	f_2	Ksv_2 (M^{-1})
No *S*-hexyl GSH	0.59	2.7 ± 0.4	0.41	0.97 ± 0.3	0.64	2.2 ± 0.3	0.36	1.3 ± 0.5
+*S*-hexyl GSH	0.49	4.3 ± 0.5	0.51	0.75 ± 0.4	0.59	7.1 ± 0.4	0.41	0.90 ± 0.5

[a] Samples were 1 μM GST, 50 mM MOPS, pH 7.5, 25 °C with no substrate or 200 μM *S*-hexyl GSH. See Materials and methods for details.
[b] The reported values are the average of three nonlinear regression analyses using different data sets fit to the equation $F/F_0 = f_1/(1 + Ksv_1[Q]) + f_2/(1 + Ksv_2[Q])$. Data from two emission wavelengths were analyzed. The same analyses at intermediate wavelengths did not yield unique solutions.

readily for both ligand states, it would be predicted that the spectrum of GST in the presence of acrylamide would be blue-shifted compared to the unquenched spectrum; this was observed experimentally for both substrate-free and *S*-hexyl GSH-bound enzyme. Because of limited instrument availability, the time-resolved quenching experiments required to confirm the prediction that the long lifetime component is quenched selectively were not performed, and bimolecular quenching constants for the individual lifetime components could not be determined. However, the recovered values for Ksv_i in Table 2 imply that the red-shifted components (Ksv_1) are quenched more easily than the blue-shifted components (Ksv_2). This difference is most dramatic in the presence of *S*-hexyl GSH.

Time-resolved anisotropy

The microconformational heterogeneity of Trp 21 and the ligand-induced conformational change in the region surrounding this residue are of particular interest when the temperature factors (crystallographic B-factors) of the mu-class enzyme are considered (Ji et al., 1992). The amino acid side chains at the C-terminal end of α-helix 1 are associated with relatively low B-factors, although the main-chain B-factors are variable in this region, with some main-chain motion implied from these crystallographic parameters. These results suggest that the region around Trp 21 is dynamic and not "conformationally locked." Therefore, we performed differential polarization measurements to determine directly the rotational correlation time(s) of the Trp 21. The phase and modulation differences between $I_\parallel$ and $I_\perp$ for 16 modulation frequencies of excitation light are shown in Figure 5. The excited-state lifetime values and fractional intensities recovered under the experimental conditions used for the anisotropy decay analysis are nearly identical to those summarized in Table 1. The minor differences presumably result from differences in instrument configuration. The anisotropy decay was assumed to be described by a sum of nonassociative anisotropy decay terms. No attempt was made to fit the data to more complex associative models in which individual anisotropy decay terms were assigned to individual excited-state lifetimes. There is a maximum phase angle difference of approx. 2°. This is a relatively small differential phase angle, but the data fit well to the sum of two exponentials with recovered rotational correlation times that clearly reflect global motion of the dimer and a fast rotational component that indicates local motion of the tryptophan side chain (Table 3). Addition of a third anisotropy decay component did not result in an improvement of the data fit, and attempts to fit the data to a single, homogeneous anisotropy decay resulted in elevation of the χ^2 value to 3.89. Although the fast correlation time is the minor component, its inclusion in the decay model improves the fit of the data significantly.

The recovered parameters for the limiting anisotropy and for the rotational motion of the dimer are in excellent agreement with expected values for tryptophan and for a protein with a molecular weight of 51,114 kDa, respectively. Rigorous error analysis of the recovered parameters indicates that the rotational correlation time attributed to local motion is well resolved at both the high

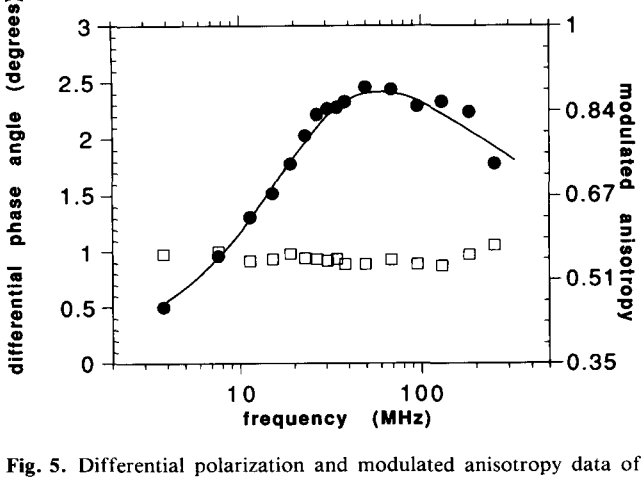

Fig. 5. Differential polarization and modulated anisotropy data of A1-1 GST. The parameters recovered from the best exponential fit of these are data are summarized in Table 3. Solid circles, differential phase angle; open squares, modulated anisotropy.

Table 3. *Fluorescence anisotropy parameters for Trp 21*

Parameter[a]	Recovered value	Expected or literature value[b]
Global χ^2	2.005	
f_1	0.354	
Lifetime t_1	5.99 ns	
f_2	0.532	
Lifetime t_2	2.78 ns	
f_3	0.114	
Lifetime t_3	0.748 ns	
r_0	0.250	0.25–0.30
r_1	0.225	
ϕ_1	26.078 ns +9.16/−5.16	25.84 ns
r_2	0.025	
ϕ_2	0.723 ns +1.80/0.07	

[a] f_1, f_2, and f_3 are the fractional intensities of the excited-state lifetimes recovered in this analysis, t_1, t_2, t_3; r_0 is the limiting anisotropy, the literature value is from Harris and Hudson (1991); r_1 and r_2 are the fractional zero-time anisotropies of the rotational correlation times, ϕ_1 and ϕ_2, obtained from g_1 and g_2, respectively.

[b] The calculated value for the rotational relaxation time corresponding to global rotation of the entire GST dimer is $r = 3(\mathrm{MW})(\nu + \delta)\eta/RT$, where MW is 51,144 g/mol dimer, ν is 0.73 mL/g, η is 1.004 cpoise, R is the gas constant, δ is the hydration state, 0.4 mL/g, and temperature T is 298 K. The rotational correlation time $\phi = r/3$.

and low limits, with a well-defined minimum. It is also important that the fractional intensities of the two rotational correlation times are resolved well by this error analysis. For example, the fraction of anisotropy decay contributed by ϕ_1 is definitely not greater than 93% of the total, and the fractional intensity of ϕ_2 is not less than 7%, although it may be as high as 15%. Although rigorous error analysis indicates that the fast rotational correlation time may be as high as 2.53 ns, it is resolved completely from the rotational correlation time associated with global rotation of the dimer. The general relation describing the anisotropy of a chromophore bound to a polymer at time t, $r(t)$, is given by Equation 1:

$$r(t) = r_0 e^{(-t/\phi_1)}[\gamma e^{(-t/\phi_2)} + (1 - \gamma)], \quad (1)$$

where r_0 is the anisotropy at time 0, γ is the fraction of total depolarization due to internal motion, and ϕ_1 and ϕ_2 are rotational correlation times of the global motion and the internal motion, respectively (Steiner, 1991). In the case where $\phi_1 \gg \phi_2$, Equation 1 reduces to:

$$r(t) = r_1 e^{-t/\phi_1} + r_2 e^{-t/\phi_2}, \quad (2)$$

where $r_2 = r_0\gamma$ and $r_1 = r_0(\gamma - 1)$. One possible simplifying model for tryptophan motion superimposed on global protein motion assumes that the internal motion approximates diffusion in a cone, where the cone semiangle θ is given by Equation 3:

$$r_1/(r_1 + r_2) = \cos^2\theta(1 + \cos\theta)^2/4. \quad (3)$$

This simple model predicts that the cone semiangle swept out by Trp 21 is 17.5° Although this tryptophan clearly exhibits local dynamics, these results indicate that it is restricted to a cone of small dimensions.

Discussion

Steady-state and time-resolved fluorescence parameters of Trp 21 in rat GST A1-1 have been determined. They indicate that when substrates or GSH conjugates bind to the H-site, this tryptophan undergoes microconformational reorganization. Together with the fluorescence anisotropy data presented here, this suggests that Trp 21 is dynamic and is in a region of the protein that is important for ligand-induced conformational change. Although no X-ray crystal structure for an alpha-class GST has been published, it is likely that the alpha-class isoenzymes are topologically very similar to the pi- and mu-class enzymes. Given the apparent structural similarity between these different isoforms of GST, these fluorescence data indicate that ligand binding to the H-site leads to detectable conformational changes not limited to the immediate vicinity of the active site.

The relatively blue-shifted emission maximum at 329 nm is typical for a tryptophan in a hydrophobic environment. The environment of Trp 21 may be inferred from the available crystal structures of the pi- and mu-class enzymes. The peptide segment flanking Trp 21 is analogous to helix 1 of the mu- and pi-class enzymes, and this Trp residue would be expected to lie between the middle of helix 1 and its C-terminus. The N-terminus of this helix forms part of a "wall" of the GSH-binding site. In the M3-3 isoenzyme, the C-terminal end of helix-1 lies 18–20 Å from the nearest atom of protein-bound GSH and therefore would not be considered to be part of the G-site. Also, the H-site, which accommodates many electrophilic hydrophobic substrates, occupies a cleft that is formed partly from the N-terminal domain and the C-terminal domain of the folded protein. The data presented here indicate that even "small" H-site ligands, such as a hexyl chain, can affect regions of the protein far from the active site of the A1-1 isoenzyme. The magnitude of ligand-induced microconformational reorganization of this end of helix 1 may vary between the isozymes of different classes, and larger substrates may induce more dramatic conformational changes than the hexyl chain of the substrate used here. For example, we have found that CDNB, a common H-site substrate, causes a marked quenching of the steady-state fluorescence of Trp 21. Although a conformational change that includes Trp 21 may occur when CDNB binds, the steady-state changes are difficult to analyze because the substrate absorbs the excitation light at 295 nm, resulting in an inner filter effect. Therefore, we chose *S*-hexyl GSH, which is spectroscopically silent in the wavelength region used here.

Two aspects of the fluorescence quenching data are particularly informative. The first regards the environment of Trp 21 in the substrate-free protein. The fact that this Trp residue is insensitive to quenching by iodide, but is readily quenched by acrylamide, suggests strongly that it is surrounded by hydrophobic residues and is not solvent accessible. Moreover, the residue analogous to Trp 21 in the M3-3 enzyme, Leu 18, clearly is surrounded by nonpolar residues including Tyr 22, Leu 19, Phe 157, Phe 187, Tyr 202, and Tyr 196, together forming a very hydrophobic patch. These residues correspond to an alanine, leucine, isoleucine, isoleucine, glutamine, and phenylalanine in the A1-1 protein, which apparently has an analogous hydrophobic patch. Therefore, this presumed location of Trp 21 readily explains the quenching data in the absence of substrate. The second noteworthy aspect of the quenching data is the difference in wavelength dependence of acrylamide quenching between the substrate-free and inhibitor-bound proteins. This clearly demonstrates a ligand-induced change in the environment of this tryptophan. It is noteworthy that several of the hydrophobic residues presumed to be in contact with Trp 21 are found in domain II of the same subunit. In fact, hydrophobic contacts between α-helix 1 of domain I and α-helices 4 and 5 of domain II are largely responsible for stabilizing the interactions between these domains of the M3-3 enzyme (Ji et al., 1992). Thus, it is reasonable to propose that some subtle rearrangement of the interface between these domains occurs when substrate binds to the H-site.

The time-resolved fluorescence data are consistent with this model. Like tryptophans in many other proteins, Trp 21 of rat A1-1 GST exhibits heterogeneous excited-state decay kinetics, and the phase and modulation data fit well to a model that includes three discrete lifetime components. We have attributed the multiple exponential decay kinetics to ground-state heterogeneity; others have done the same for single tryptophan proteins (Royer et al., 1990; Stayton & Sligar, 1991). Such heterogeneity is common, although examples of homogeneous fluorescence decay have been reported (Hutnik & Szabo, 1989). Upon addition of *S*-hexyl GSH to rat A1-1 GST, the contribution of the short lifetime component of Trp 21 is reduced dramatically, and the fractional intensity of the longest lifetime component is increased correspondingly. The wavelength dependence of each of the lifetime components also provides a useful spectroscopic probe (SAS, Fig. 3). The median lifetime component is significantly blue-shifted relative to the long lifetime component, whereas the short component exhibits little wavelength dependence. In this regard, the time-resolved data and the steady-state quenching data provide an internally consistent model for Trp 21 and the change in environment that it undergoes upon addition of *S*-hexyl GSH.

The anisotropy data add to the dynamic model of Trp 21, indicating clearly that this residue exhibits local motion at 25 °C. Many buried tryptophans exhibit "gated" local motion, i.e., the rotational or segmental motion is observed only at elevated temperatures at which neighboring residues are expected to become more dynamic, or at elevated pressures that lead to unfolding (Harris & Hudson, 1991; Royer et al., 1993). Increased thermal fluctuation results in transient removal of the steric hindrance that prevents local motion of some residues at lower temperatures. Although Trp 21 is apparently partially buried, the local motion of this residue is detected easily. If the motion of this tryptophan is assumed to approximate rotation from an anchored peptide segment about an axis that defines a cone superimposed on the global rotation of the dimer, then the cone angle swept out by this local rotation is 17.5° (see Results). This simplifying model suggests that, although Trp 21 exhibits local motion, it is restricted to a narrow range of accessible microconformations. The crystallographic B-factors of the M3-3 enzyme suggest that the analogous side chain, Leu 18, lies within a region that has some local mobility, although it is clearly not as dynamic as the residues in helices 4 and 5a, or in the C-terminal tail. In this regard, the data presented here provide additional evidence that the A1-1 GST is similar, topologically and dynamically, to the pi- and mu-class enzymes.

It is significant that GSH does not induce the spectral changes that are observed when *S*-hexyl GSH binds to the rat A1-1 GST. This implies that occupation by a substrate of the H-site, rather than the G-site, is required for these conformational changes. It also is possible that these spectral changes reflect conformations attained during the transition state and maintained in the product, GSH–conjugate complex. The fact that CDNB also causes changes in the spectrum of Trp 21 in the absence of GSH indicates that these conformational changes are not limited to transition states or product complexes. Comparison of the porcine pi-isoenzyme bound to GSH sulfonate (Reinemer et al., 1991) with the human pi-enzyme that has *S*-hexyl GSH bound (Reinemer et al., 1992) suggests that no global domain movement or dramatic reorganization takes place when the *S*-hexyl moiety is added to the H-site. However, careful inspection of these structures does reveal that the C-terminal end of helix 1 is displaced slightly in these superimposed structures. Structural differences between the substrate-free and ligand-bound enzyme may be important for catalytic function. In fact, recently we have demonstrated that the evolutionarily conserved catalytic tyrosine at the active site of substrate-free rat A1-1 GST has an unusually low pK_a which increases in the presence of *S*-hexyl GSH (Atkins et al., 1993). The catalytic advantage for an active-site tyrosine with a low pK_a in reactions mediated by GSTs has been discussed (Reinemer et al., 1991; Ji et al., 1992). Presumably, specific structural features of the substrate-free protein contribute to the ionization behavior of this residue, and ligand-induced structural changes may modulate this pK_a.

Materials and methods

Enzyme purification

Reduced GSH and *S*-hexyl GSH were obtained from Sigma (St. Louis, Missouri) and were used without further purification. Recombinant rat GST A1-1 was obtained from *Escherichia coli* cultures (strain AB 1899) harboring the expression vector pKK 2.7 with the GST-encoding fragment cloned into the EcoR I and Sal I sites (Wang et al., 1992b). Cells from an 8-L culture were harvested by centrifugation at 8,000 × *g* for 20 min and disrupted by sonication in 10 mM sodium phosphate buffer, pH 7.4, containing 5 mM EDTA. After centrifugation at 100,000 × *g* for 60 min, the cytosolic fraction was concentrated and subjected to gel filtration with Sephadex G-50. The fractions containing GST activity were pooled and loaded onto a *S*-hexyl GSH-epoxy-agarose (Sigma) column equilibrated with 25 mM Tris-HCl, pH 8.0. The GST was eluted with 2.5 mM GSH and 5 mM *S*-hexyl GSH. The final preparation had a specific activity in the CDNB assay of 48 μmol/min/mg.

Steady-state fluorescence

Steady-state fluorescence experiments were performed on an SLM-Aminco 8000C fluorometer. Samples typically contained 1 μM GST, 50 mM MOPS, pH 7.5. Spectral bandpasses were 4 nm for all steady-state experiments. No polarizers were used in steady-state measurements. Although it is conceivable that the absence of polarizers in quenching experiments leads to small systematic errors, it is unlikely that this accounts for the observed differences in substrate-free and ligand-bound GST. For iodide quenching experiments, samples with varying concentrations of iodide were kept at constant ionic strength by addition of an appropriate concentration of KCl. The Stern–Volmer quenching constants for the individual lifetime components were obtained from the relationship $F/F_0 = \sum f_i/(1 + [Q]Ksv_i)$, where F_0 and F are the wavelength-dependent fluorescence intensities in the absence and presence of quencher, respectively, Q is the concentration of quencher, f_i is the fractional intensity of the ith component, and Ksv_i is the Stern–Volmer quenching constant of the ith component (Eftink [1991] and references therein). Nonlinear regression utilizing this equation was accomplished with the software package Enzfitter®. Blank spectra (buffer only) were subtracted from all sample spectra. All spectra are the average of at least three emission scans.

Fluorescence lifetime measurements

Multifrequency phase and modulation experiments were performed at the Laboratory for Fluorescence Dynamics, University of Illinois, Urbana, Illinois. The instrument utilizes cross-correlation detection. Excitation at 295 nm was achieved with a frequency-doubled (532 nm), modelocked (38 MHz) neodynium-YAG laser synchronously pumping a cavity-dumped, rhodamine 6G dye laser (Coherent Corp, Palo Alto, California). Emission was detected through band-pass filters (320, 330, 340, 360, and 380 nm; 8–10 nm band pass). For intensity decay measurements, "magic angle" conditions were satisfied by placing polarizers in both excitation and emission light paths. The orientation of the excitation polarizer was offset from the emission polarizer by 55°. The instrument is essentially as described elsewhere (Alcala et al., 1987). *p*-Terphenyl in ethanol was used as a standard with an excited-state lifetime of 1.05 ns. Differential polarization measurements were performed on the same instrument, utilizing T-format detection. Excitation light was polarized vertically, and the phase angle difference between the parallel and perpendicular emission components was determined. Emission in both channels was through a TG-350 bandpass filter (40 nm band pass) and a WG-305 UV cutoff filter. Lifetime measurements of the same samples were performed with these same filters immediately prior to measurement of the differential phases and modulated anisotropy ratios.

Data analysis

Fluorescence intensity decay data were analyzed with the software Globals Unlimited® (Knutson et al., 1983; Beechem et al., 1991). The relations used to calculate excited-state lifetimes, t, from the phase angles, f, and demodulation factors, m, are: $\tan \phi = \omega\tau$ and $m = (B/A)(b/a) = (1 + \omega^2\tau^2)^{-1/2}$, where $\omega = 2\pi \times$ frequency in hertz, and B/A, b/a are the modulated intensity ratios. Anisotropy data were analyzed as the sum of exponentials, according to $r(t) = r_0 \sum g_i e^{-t/\phi_i}$, where $r(t)$ and r_0 are the anisotropy of the ith component at time = t and $t = 0$, respectively. Here, g_i is the fractional intensity of the ith anisotropy decay component, and ϕ_i is the rotational correlation time of the ith component. The global analysis utilizes a Marquardt–Levenberg nonlinear least-squares global matrix to link experimentally measured parameters. The theory and philosophy of the rigorous error analysis provided by this software have been described previously (Beechem et al., 1991). It is essential to note that errors reported in the tables are not standard deviations for individual measurements, but confidence limits resulting from a χ^2 minimization when a specific parameter is varied and others are fixed. The errors therefore do not provide a measure of the precision of the values, but rather a rigorous measure of the confidence associated with a specific recovered value within the constraints of the fixed parameters in a specific model. The precision of the measurements is: phase angles <0.6° and modulation ratio <0.004.

Molecular modeling

Structural analysis of the M3-3 GST was accomplished with the software package Quanta® and a Silicon Graphics 4D-20 workstation.

Note added in proof

While this manuscript was in press, the X-ray crystal structure of human A1-1 GST, with *S*-phenyl GSH bound, was published (Sinning et al., 1993). This structure indicates that Trp 21 lies in a hydrophobic region between domains of the individual subunits.

Acknowledgments

We acknowledge Drs. Chip Hazlett and Enrico Gratton for assistance in performing the time-resolved experiments and for many helpful discussions.

References

Alcala, J.R., Gratton, E.R., & Prendergast, F.G. (1987). Interpretation of fluorescence decays in proteins using continuous lifetime distributions. *Biophys. J. 51*, 925-936.

Armstrong, R.N. (1991). Glutathione-*S*-transferases: Reaction mechanism, structure, and function. *Chem. Res. Toxicol. 4*, 131-140.

Atkins, W.M., Wang, R.G., Newton, D.J., Bird, A.W., & Lu, A.Y.H. (1993). The catalytic mechanism of glutathione *S*-transferase: Spectroscopic determination of the pKa of Tyr-9 in rat a 1-1 GST. *J. Biol. Chem. 268*, 19188-19191.

Beechem, J.M., Gratton, E., Ameloot, M., Knutson, J.R., & Brand, L. (1991). The global analysis of fluorescence intensity and anisotropy decay data: Second generation theory and programs. In *Topics in Fluorescence Spectroscopy*, Vol. 2 (Lakowicz, J., Ed.), pp. 241-301. Plenum Press, New York.

Beechem, J.M., Knutson, J.R., Ross, J.B., Turner, B.W., & Brand, L. (1983). Global resolution of heterogeneous decay by phase/modulation fluorometry: Mixtures and proteins. *Biochemistry 22*, 6054-6058.

Caccuri, A.M., Aceto, A., Rosato, N., Di Ilio, C., Piemonte, F., & Federici, G. (1991). Intrinsic fluorescence quenching of glutathione transferase p by glutathione binding. *Ital. J. Biochem. 40*, 304-311.

Coles, B. & Ketterer, B. (1990). The role of glutathione and glutathione transferases in chemical carcinogenesis. *CRC Crit. Rev. Biochem. Mol. Biol. 25*, 47-67.

Eftink, M.R. (1991). Fluorescence quenching: Theory and applications. In *Topics in Fluorescence Spectroscopy*, Vol. 2 (Lakowicz, J., Ed.), pp. 53-120. Plenum Press, New York.

Graminski, G.F., Kubo, Y., & Armstrong, R.N. (1989). Spectroscopic and kinetic evidence for the thiolate anion of glutathione at the active site of glutathione-*S*-transferase. *Biochemistry 28*, 3562-3568.

Harris, D.L. & Hudson, B.S. (1991). Fluorescence and molecular dynamics study of the internal motion of the buried tryptophan in bacteriophage T4 lysozyme: Effects of temperature and alteration of nonbonded networks. *Chem. Physics 158*, 353-383.

Hutnik, C.M. & Szabo, A.G. (1989). A time-resolved fluorescence study of azurin and metalloazurin derivatives. *Biochemistry 28*, 3935-3939.

Ji, X., Zhang, P., Armstrong, R.N., & Gilliland, G.L. (1992). The three-dimensional structure of glutathione *S*-transferase from the mu gene class. Structural analysis of the binary complex of isoenzyme 3-3 and glutathione at 2.2 Å resolution. *Biochemistry 31*, 10169-10184.

Knutson, J.R., Beechem, J.M., & Brand, L. (1983). Simultaneous analysis of multiple fluorescence decay curves: A global approach. *Chem. Phys. Lett. 102*, 2501-507.

Kong, K.-H., Inoue, H., & Takahashi, K. (1993). Site-directed mutagenesis study on the roles of evolutionally conserved aspartic acid residues in human glutathione *S*-transferase P1-1. *Protein Eng. 6*, 93-99.

Lakowicz, J.R. (1989). Principles of frequency-domain fluorescence spectroscopy and applications to protein fluorescence. In *Cell Structure and Function by Microspectrofluorometry*, pp. 163-183. Academic Press, New York.

Liu, S., Zhang, P., Ji, X., Johnson, W.W., Gilliland, G.L., & Armstrong, R.N. (1992). Contribution of tyrosine 6 to the catalytic mechanism of isoenzyme 3-3 of glutathione *S*-transferase. *J. Biol. Chem. 267*, 4296-4300.

Mannervik, B. (1985). The isoenzymes of the glutathione transferases. *Adv. Enzymol. Mol. Biol. 57*, 357-394.

Mannervik, B. & Danielson, U.H. (1988). Glutathione-*S*-transferases: Structure and catalytic activity. *CRC Crit. Rev. Biochem. 23*, 283-337.

Meyer, D.J., Coles, B., Pemble, S.E., Gilmore, K.S., Fraser, G.M., & Ketterer, B. (1991). Theta, a new class of glutathione transferases purified from rat and man. *Biochem. J. 274*, 409-414.

Nishihara, J., Ishibashi, T., Sakai, M., Nishi, S., & Kumazaki, T. (1992). Evidence for the involvement of tryptophan 38 in the active site of glutathione *S*-transferase p. *Biochem. Biophys. Res. Commun. 185*, 1069-1077.

Penington, C.J. & Rule, G.S. (1992). Mapping the substrate-binding site of a human class mu glutathione transferase using nuclear magnetic resonance spectroscopy. *Biochemistry 31*, 2912-2920.

Pickett, C.B. & Lu, A.Y.H. (1989). Glutathione *S*-transferases: Gene structure, regulation, and biological function. *Annu. Rev. Biochem. 58*, 743-764.

Reinemer, P., Dirr, H.W., Ladenstein, R., Huber, R., Lo Bello, M., Federici, G., & Parker, M. (1992). Three-dimensional structure of class p glutathione *S*-transferase from human placenta in complex with *S*-hexyl glutathione at 2.8 Å resolution. *J. Mol. Biol. 227*, 214-226.

Reinemer, P., Dirr, H.W., Ladenstein, R., Schaffer, J., Gallay, O., & Huber, R. (1991). The three-dimensional structure of class p glutathione *S*-transferase in complex with glutathione sulfonate at 2.3 Å resolution. *EMBO J. 10*, 1997-2005.

Royer, C., Gardner, J., Beechem, J.M., Brochon, J.C., & Mathews, K.S. (1990). Resolution of the intrinsic fluorescence decay kinetics of the two tryptophan residues of *E. coli lac* repressor using genetically engineered single tryptophan mutants. *Biophys. J. 58*, 363-373.

Royer, C.A., Hinck, A.P., Loh, S.N., Prehoda, K.E., Peng, X., Jonas, J., & Markley, J.L. (1993). Effects of amino acid substitutions on the pressure denaturation of staphylococcal nuclease as monitored by fluorescence and nuclear magnetic resonance spectroscopy. *Biochemistry 32*, 5222-5232.

Sinning, I., Kleywegt, G.J., Cowan, S.W., Reinemer, P., Dirr, H.W., Huber, R., Gilliland, G.L., Armstrong, R.N., Ji, X., Board, P.G., Olin, B., Mannervik, B., & Jones, T.A. (1993). Structure determination and refinement of human alpha class glutathione transferase A1-1, and a comparison with the mu and pi class enzymes. *J. Mol. Biol. 232*, 192-212.

Stayton, P.S. & Sligar, S.G. (1991). Structural microheterogeneity of a tryptophan residue required for efficient biological electron transfer between putidaredoxin and cytochrome P450cam. *Biochemistry 30*, 1845-1851.

Steiner, R.F. (1991). Fluorescence anisotropy: Theory and applications. In *Topics in Fluorescence Spectroscopy*, Vol. 2 (Lakowicz, J., Ed.), pp. 1-51. Plenum Press, New York.

Wang, R.W., Newton, D.J., Huskey, S.-E.W., McKeever, B.M., Pickett, C.B., & Lu, A.Y.H. (1992a). Site directed mutagenesis of glutathione *S*-transferase YaYa. Important roles for tyrosine 9 and aspartic acid 101 in catalysis. *J. Biol. Chem. 267*, 19866-19871.

Wang, R.W., Newton, D.J., Pickett, C.B., & Lu, A.Y. (1992b). Site directed mutagenesis of glutathione *S*-transferase YaYa: Functional studies of histidine, cysteine, and tryptophan mutants. *Arch. Biochem. Biophys. 297*, 86-91.

Zhang, P. & Armstrong. R.N. (1990). Construction, expression, and preliminary characterization of chimeric class m glutathione *S*-transferases with altered catalytic properties. *Biopolymers 29*, 159-169.